ORIGINAL RESEARCH

Improving the Thrombocytopenia Adverse Reaction of Belinostat Using Human Serum Albumin Nanoparticles

Jia-Yu Liu[1], Chia-Hung Yen ⓘ[2,3], Ya-Fan Lin ⓘ[4], Yin-Hsun Feng[5], Yi-Ping Fang ⓘ[1,6,7]

[1]School of Pharmacy, College of Pharmacy, Kaohsiung Medical University, Kaohsiung, Taiwan; [2]Graduate Institute of Natural Products, College of Pharmacy, Kaohsiung Medical University, Kaohsiung, Taiwan; [3]Drug Development and Value Creation Research Center, Kaohsiung Medical University, Kaohsiung, Taiwan; [4]Department of Chemistry, National Dong Hwa University, Hualien, Taiwan; [5]Division of Hematology and Oncology, Department of Internal Medicine, ChiMei Medical Center, Tainan, Taiwan; [6]Regeneration Medicine and Cell Therapy Research Center, College of Medicine, Kaohsiung Medical University, Kaohsiung, Taiwan; [7]Department of Medical Research, Kaohsiung Medical University Hospital, Kaohsiung Medical University, Kaohsiung, Taiwan

Correspondence: Yi-Ping Fang, School of Pharmacy, College of Pharmacy, Kaohsiung Medical University, 100, Shih-Chuan 1st Road, San Ming District, Kaohsiung, 80708, Taiwan, Tel +886 7 3121101 ext. 2261, Email ypfang@kmu.edu.tw

Background: Belinostat, a histone deacetylase inhibitor used for hematological cancer treatments, however, it caused thrombocytopenia, poor solubility, and rapid clearance. To mitigate these issues, human serum albumin (HSA) was utilized as the core material for its high protein binding affinity and self-binding capabilities. The study focused on developing belinostat-loaded HSA nanoparticles to improve solubility, extend circulation time, and reduce adverse effects.

Methods: Belinostat-loaded HSA nanoparticles were synthesized using a desolvation method, optimized for size, charge, and entrapment efficiency, and characterized by molecular docking and Fourier-transform infrared spectroscopy (FTIR). Cytotoxicity was assessed in vitro against HuT-78 cells, and in vivo pharmacokinetics and toxicology studies were conducted to evaluate therapeutic efficacy and safety.

Results: The prepared belinostat–HSA nanoparticles exhibited the size of 150 nm with a charge of ~-50 mV and a high entrapment efficiency (90%). Molecular docking confirmed that belinostat and HSA had a strong binding affinity (-9.5 kcal mol^{-1}), and the entrapment of belinostat within HSA nanoparticles was also confirmed via FTIR. Belinostat–HSA nanoparticles were cytotoxic against HuT-78 with the dose–response relation (1–100 μM). The highly concentrated (100 μM) belinostat–HSA nanoparticles maintained the viability of the peripheral blood mononuclear cells with 50% survival, which did not survive when exposed to belinostat (100 μM). The belinostat–HSA nanoparticles proved suitable for intravenous administration without causing hemolysis, exhibited prolonged circulation times, and improved in vivo platelet counts significantly ($p < 0.05$).

Conclusion: In conclusion, the belinostat-loaded HSA nanoparticles significantly enhance the solubility and half-life of belinostat, reduce its adverse hematological effects, and maintain sustained drug release. These attributes underscore the potential of belinostat-HSA nanoparticles as a viable intravenous option for the treatment of hematological malignancies.
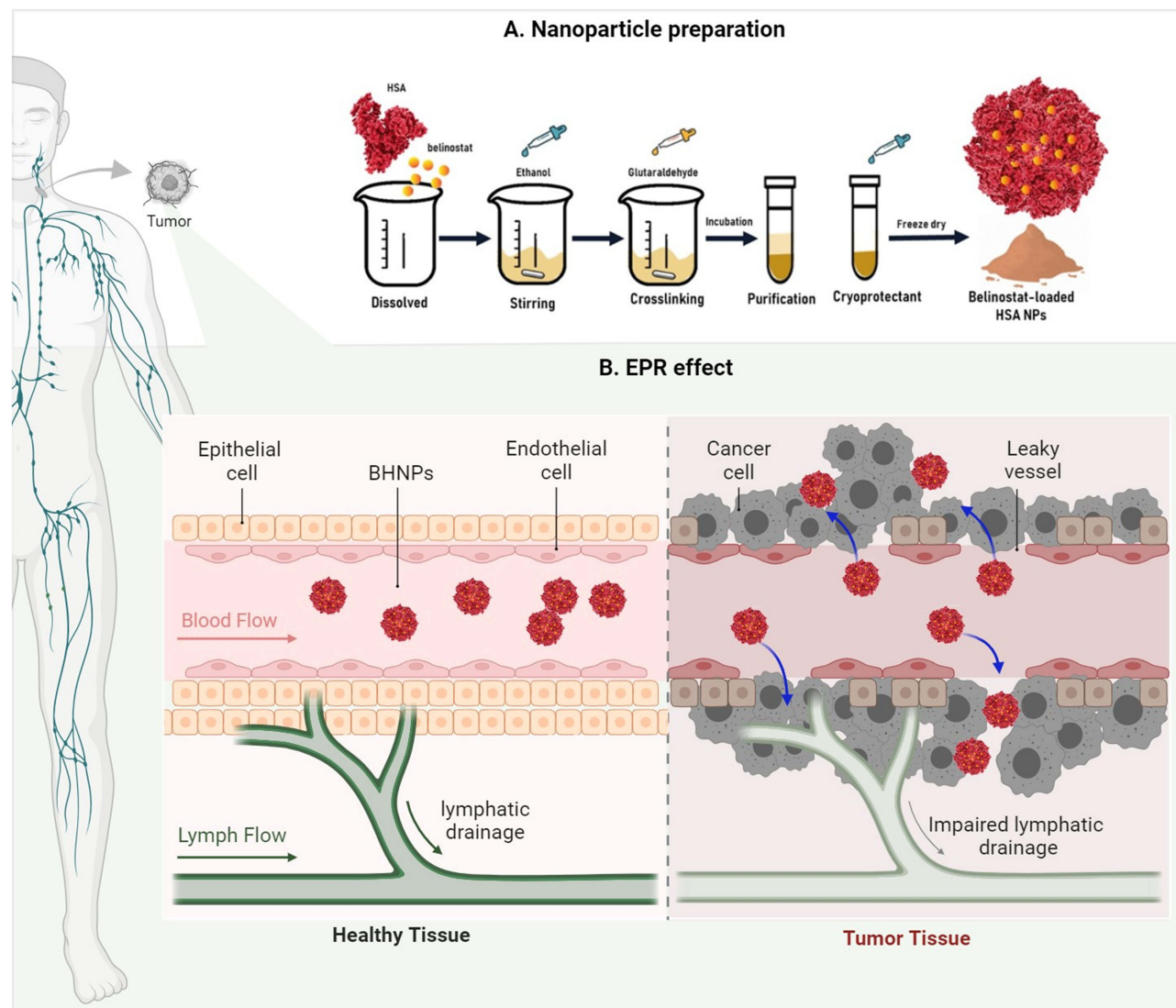
Keywords: belinostat, human serum albumin nanoparticles, peripheral T-cell lymphoma, thrombocytopenia, pharmacokinetics

Introduction

Peripheral T-cell lymphoma (PTCL), a rare and heterogeneous disease, is a type of non-Hodgkin's lymphoma. PTCL has a broad cytological spectrum, with nodal and extranodal distribution (bone marrow, peripheral blood, liver, spleen, and skin).[1] The diagnosis of PTCL is complex owing to several subtypes. Cyclophosphamide, doxorubicin, vincristine, and prednisone (CHOP) chemotherapy or CHOP-like regimens are used as the front-line treatment for PTCL, which are associated with a high failure rate and frequent relapses.[2]

Histone deacetylase (HDAC) inhibitors are a new-generation anticancer drug to treat hematological cancers. HDAC inhibitors induce cancer cell cycle arrest, differentiation, and cell death; reduce angiogenesis; and modulate immune

10785

Graphical Abstract

A. Nanoparticle preparation

HSA — belinostat — Ethanol — Glutaraldehyde — Incubation — Freeze dry — Belinostat-loaded HSA NPs

Dissolved — Stirring — Crosslinking — Purification — Cryoprotectant

B. EPR effect

Healthy Tissue: Epithelial cell, BHNPs, Endothelial cell, Blood Flow, Lymph Flow, lymphatic drainage

Tumor Tissue: Cancer cell, Leaky vessel, Impaired lymphatic drainage

response.[3] Presently, four drugs are approved by the United States Food and Drug Administration (FDA): (i) suberoylanilide hydroxamic acid (SAHA) (vorinostat, Zolinza®) and (ii) FK228 (romidepsin, Istodax®) against cutaneous T-cell lymphoma, (iii) belinostat (Beleodaq®) against refractory or regressed PTCL, and (iv) panobinostat (Farydak®) against multiple myeloma.[4] Several reports indicate promising synergistic effects by combining HDAC inhibitors with other anticancer drugs and/or radiotherapy.[5]

The major issue with HDAC inhibitors is poor solubility and a short half-life in plasma. Moreover, HDAC inhibitors have hematological and cardiotoxicity depending on the administrated doses. Belinostat (PXD101) has a low molecular weight (318.35 g mol^{-1}) and water solubility (0.14 mg mL^{-1}). The log P (1.83) of belinostat suggests that unionized belinostat is not lipophilic to extensively distribute into tissues.[6] Moreover, pKa (7.87) and high protein binding affinity (92.9–95.8%) limit the distribution.[7]

Presently, nanomedicines are considered as a new treatment strategy. Nanotechnology enhances the therapeutic outcome by solving drug-delivery issues. Previous reports indicate the use of various potential carriers to deliver HDAC inhibitors such as liposomes,[8] micelles,[9] hyaluronic acid–coated solid lipid nanoparticles,[10] all-trans retinoic

acid nanoparticles,[11] polymeric nanocarrier,[12] aminoglycoside-derived lipopolymers nanoparticles,[13] and pH-sensitive polymeric nanoparticles.[14]

The nanomedicines approved by the FDA and European Medicines Agency such as liposomes, lipid and inorganic nanoparticles, and albumin particles[15] are based on different delivery strategies. Although liposome is the major and oldest platform, human serum albumin is another candidate. HSA is an easily available biomimetic material with high biocompatibility and low toxicity.[16] HSA, a water-soluble protein, has a molecular weight of 66.5 kDa comprising 585 amino acids. The structure includes three stereospecific domains: I, II, and III.[17] HSA, comprising 17 pairs of disulfide bridges and a free cysteine (Cys 34) residue, is easy to fabricate and provides a conjugate site for drugs.[18] The surface charge of albumin can be easily controlled by modulating the pH environment based on the isoelectric point of 4.7 (Γ/2 = 0.15) or 5.2 (Γ/2 = 0).[19] Albumin-based nanomedicines can be loaded with any active components via a simple click chemistry process.[20] HSA present in human blood is biocompatible and biodegradable with low immunogenic properties and is suitable as drug-delivery carriers.[21] The HSA structure can be prepared feasibly at different geometric nanometer scales owing to the particle confinement effect. The outer surface of HSA can be modified via grafting, which shows improved light and heat characteristics. Albumin prolongs the half-life circulation when conjugated with binders or nanoparticles. Hence, albumin is suitable as sustained and prolonged release material. Albumin is highly absorbed and metabolized by rapidly growing and nutrient-starved cancer cells.[22] The albumin-based drug-delivery system has specific characteristics, which can be used in lymphatic target delivery. HSA nanoparticles can be effective for delivering therapeutic agents via the lymphatic system due to the several pre-dominant factors. HSA nanoparticles in the 10–100 nm range are too large to cross the blood capillary endothelium, enabling efficient transport through lymphatic vessels. Additionally, albumin naturally exits blood capillaries and is absorbed into lymphatic vessels, allowing HSA nanoparticles to "hitchhike" on this natural pathway, enhancing lymphatic targeting. The movement of interstitial fluid toward the lymphatics also drives the convective flow that transports both albumin and HSA nanoparticles, ensuring uptake efficiently.[23,24] Currently, two FDA-approved commercial components are available: (i) Abraxane® (paclitaxel protein-bound particles for injectable suspension) as a drug-delivery system for the treatment of metastatic breast cancer and the first-line treatment of locally advanced or metastatic non-small cell lung cancer[25] and (ii) Technetium-99m-labeled HSA (99mTc-HSA) used as a blood pool imaging agent.[26]

Although extensive studies report using nanotechnology concepts, clinical hematological and cardiac toxicity exist with increased administered doses. Thus, we used the high protein binding property of belinostat to self-bind with assembled HSA NPs (HNPs) to investigate the possibility of prolonging the half-life and improving the safety. We optimized and characterized the belinostat-HNPs (BHNPs) formulation. The possible binding interaction was character-ized via Fourier-transform infrared (FTIR) spectroscopy and molecular docking. The antitumor activity and specific targeting ability of the sample were tested on Hut-78 and peripheral blood mononuclear cells (PBMC). In addition, in vivo toxicity and pharmacokinetics were assessed.

Materials and Methods
Materials
Belinostat was purchased from Active Biochem (HK). HSA lyophilized powder (≥96% pure) was purchased from Sigma–Aldrich (St. Louis, MO, USA). Glutaraldehyde was purchased from AppliChem GmbH (Darmstadt, German). Ethanol and acetonitrile (analytical reagent grade) were obtained from Mallinckrodt (Staines-upon-Thames, UK). Iscoves's modified Dulbecco's medium (IMDM), Roswell Park Memorial Institute (RPMI) 1640 medium, and fetal bovine serum (FBS) were obtained from Gibco (New York, NY, USA). All other reagents used were of the analytical grade. The procedures on Sprague–Dawley rats were performed with the approval of the Institutional Committee for the Care and Use of Animals Kaohsiung Medical University (IACUC approval No: 108268), Kaohsiung, Taiwan. All animal experiments and related procedures were conducted in accordance with the ordinances of the Ministry of Health and Welfare, Taiwan.

Preparation of Belinostat-Loaded HSA Nanoparticles (BHNPs)

BHNPs were prepared using the desolvation method. Specific amounts of HSA lyophilized powder were dissolved in 1-mL ultrapure water. Belinostat was added to the solution after HSA powder was completely dissolved. When prepared empty HNPs without incorporating belinostat. Anhydrous ethanol was added to the solution with a controlled flow rate of 0.5 mL min^{-1} under stirring at 550 rpm, followed by the addition of 8% glutaraldehyde with a controlled flow rate of 1 mL min^{-1} with stirring.[27] The mixture was stirred for 24 h. The crosslinked suspension was purified using three cycles of centrifugation and dispersion, which was finally dispersed in 1-mL phosphate-buffered saline (PBS) (pH 7.4). The stability of the freeze-dried sample was evaluated. Three percent sucrose or trehalose were added to a fresh BHNP suspension as cryoprotectants. The cryoprotectant was added in the final step, which was dispersed in PBS. The fresh HSA suspension was stored at −20 °C for 4–6 h, followed by freezing at −80 °C overnight. The sample was lyophilized for 24 h under freeze conditions to obtain a fine powder. The preparation procedure of BHNPs is shown in Figure 1.

Validation of Belinostat via High-Performance Liquid Chromatography (HPLC)

Belinostat was analyzed via high-performance liquid chromatography (HPLC). The HPLC system comprises an L-7100 pump, L-7200 autosampler, L-7455 diode array detector at 265 nm (Hitachi, Tokyo, Japan), and a Purospher Star RP-18 end-capped column (250 mm × 4.6 mm, internal diameter = 5 μm, Merck). The mobile phase consists of a water phase (water with 0.1% Phosphoric acid) and organic phase (acetonitrile). The gradient elution was programmed as follows: 0–-6 min, 100% water phase (A); 6–9 min, 5% water phase, 95% organic phase; 9–10 min, 5% water phase, 95% organic phase; 10–15 min, 100% water phase. The mixture was separated via gradient elution with a flow rate of 1 mL min^{-1}. The column oven was set at 30 °C. The limits of detection and quantitation of belinostat were determined by dissolving belinostat in distilled deionized water with decreasing concentrations until the signal/noise ratios were 3 and 10. The linearity of the standard curves, intraday and interday precisions, and accuracy were established. The retention time was 8.24 min.

Characterization of the Particle Diameter and Zeta Potential

The particle diameter (d) and zeta potential (ζ) of HNPs or BHNPs were measured via dynamic light scattering (DLS) (ELSZ-2000, Otsuka Electronic, Hirakata, Japan). The polydispersity index (PDI) was used to measure the size distribution. All HNPs or BHNPs were diluted 20-fold with double-distilled water to achieve the count rate for measurements. The measurements were repeated thrice for each of the three samples.

Measurement of Encapsulation Efficiency

The BHNPs were centrifuged at 80,000 relative centrifugal force (RCF) for 30 min to separate nonbonded belinostat. The supernatant was dried overnight and redispersed in double-distilled water for HPLC analysis. The encapsulation efficiency of HNPs was calculated using Equation (1).
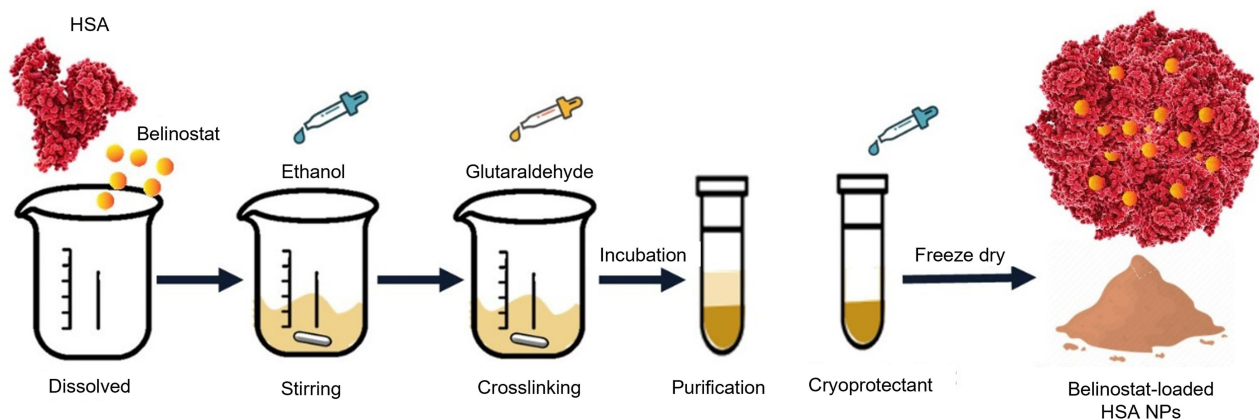

Figure 1 Schematic representation of the preparation of BHNPs.

10788

DovePress

International Journal of Nanomedicine 2024:19

$$\text{Encapsulation efficiency (\%)} = \frac{Total\ amount\ of\ belinostat - amount\ of\ belinostat\ in\ the\ supernatant}{Total\ amount\ of\ belinostat} \times 100\%, \quad (1)$$

where the total amount of belinostat is the amount of drug placed in the HNP formulation, and the amount of belinostat in the supernatant is the supernatant collected after centrifugation.

Morphology

The structure and morphology of the samples were analyzed via scanning electron microscopy SEM (JSM-5300, SEM JEOL, Japan) and transmission electron microscopy (TEM) (JEM-1400; JEOL, Tokyo, Japan). The BHNP suspension was added dropwise onto a Formvar/carbon film on a 200-mesh copper grid (FCF-200-Cu; Electron Microscopy Sciences, Hatfield, PA, USA) and stained with 1% phosphotungstic acid for 1 min. After negative staining, the sample was washed with distilled deionized water. The sample was dried under vacuum overnight and analyzed via TEM.

FTIR Spectroscopy

The samples were diluted with 1% KBr powder, pressed into 16-mm disks at 15 t, and analyzed using a FTIR spectrometer (Vertex 70 v, Bruker, Billerica, USA). The wavenumbers ranged from 4000 cm^{-1} to 380 cm^{-1} at a resolution of 1 cm^{-1}.

Molecular Docking

The molecular structure of belinostat was created via the ChemDraw Professional 17.0 software, followed by geometrical optimization via MMFF94 force field in Chem3D 17.0. The optimal belinostat file was converted into the suitable PDBQT format for docking simulation. The crystal structure of HSA (PDB code: 1bj5) with 1.90 Å resolution was retrieved from the RCSB Protein Data Bank (PDB). Following the removal of water, hydrogenation occurred. The PDBQT format of modeling the 3D structure was generated using AutodockTools-1.5.6 package.

The theoretical binding energy between belinostat and the HSA receptor was calculated using the Autodock Vina software. The docking calculation was performed by setting the HSA receptor as a rigid body and allowing the belinostat ligand to rotate around single bonds. The interaction energy was calculated by considering belinostat and HSA within a cubical grid box centered at the binding pocket of HSA, setting the grid spacing as 1.00 Å, and the grid box size as 100 Å × 84 Å × 90 Å. The resulting docking structure was analyzed using the Discovery Studio Client v19.1.0.18287 software.

Cell Cytotoxicity

The cutaneous T-cell lymphoma cell line (HuT-78) was purchased from the Bioresource Collection and Research Center (Hsinchu, Taiwan). HuT-78 cells were incubated in 79% IMDM with 20% FBS and 1% liquid penicillin–streptomycin. The mixture was allowed to stand in a humidified atmosphere containing 5% CO_2 at 37 °C. HuT-78 cells were seeded on a 96-well culture plate at a cell density of 1×10^4 cells per well. The medium contained a free belinostat drug or belinostat in ethanol, HNPs only and BHNPs at final concentrations of 0.1–10 μM for 24, 48, and 72 h. The samples were incubated overnight. The incubated cells were reacted with 10-μL Cell Counting Kit-8 (CCK-8, Enzo, Farmingdale, NY, USA) for 2 h. The absorbance was recorded at 450 nm using an enzyme-linked immunosorbent assay reader (BioTek Epoch; Thermo Fisher Scientific, Waltham, MA, USA) to measure the quantity of surviving cells. The half-maximal inhibitory concentration (IC_{50}) was calculated using GraphPad. The cell cytotoxicity was calculated using Equation (2).

$$Cell\ viability\ (\%) = \frac{Ab_{sample} - Ab_{blank}}{Ab_{control} - Ab_{blank}} \times 100\%, \quad (2)$$

where Ab denotes absorbance, $Ab_{control}$ represents 100% survival, and Ab_{blank} represents no cells.

Ex vivo Hemolysis Assay

Red blood cells (RBCs) were collected from male Sprague–Dawley rats. The blood sample was collected through VACUTAINER™ tubes, centrifuged at 2000 RCF for 10 min, followed by dispersion in PBS [pH 7.4, 1:9 (v/v)] as the

stock solution, and stored at 4 °C. The process was repeated thrice. Hemolysis was analyzed by preparing the sample as mentioned. 100-µL stock solution was mixed with 50-µL free belinostat, HNP, BHNP formulations, and 2.45-mL PBS (pH 7.4). The mixture was incubated at 37 °C for 1 h and centrifuged at 2000 RCF for 5 min. The supernatant was assayed at 415 nm using a UV spectrometer. The measured value for the positive control was RBC dissolved in water (100% hemolysis), while the value for the negative control was RBC dissolved in PBS (pH 7.4; 0% hemolysis). The hemolysis percentage was calculated using Equation (3), where X is the value of hemoglobin.

$$\text{Hemolysis } (\%) = \frac{X - Control_{PBS}}{Control_{H_2O}} \times 100\%. \tag{3}$$

Ex vivo of Peripheral Blood Mononuclear Cells (PBMCs) Assay

PBMCs were isolated from the peripheral blood collected from male Sprague–Dawley rats. PBMCs were isolated using the density gradient centrifugation method by Ficoll–Paque™ PLUS (GE, Healthcare, Uppsala, Sweden). PBMCs were collected from the interphase layer and washed thrice with an RPMI 1640 medium. PBMCs (1 x 10^6 cells/well) were seeded using a 96-well plate and incubated at 37 °C in the presence of 5% CO_2 and RPMI 1640 with 10% FBS. Cytotoxicity assay was conducted after the samples were incubated overnight. The procedure was the same with Method 4.10.

In vivo Pharmacokinetic Study

An in vivo pharmacokinetic study was conducted on healthy male Sprague–Dawley rats of ~300 g from BioLASCO (Taipei, Taiwan). Sprague–Dawley rats were anesthetized using Zoletil® intramuscular injections administrated at 0.4 mg kg^{-1} and randomly divided into two groups: belinostat control (belinostat dissolved in a 10% ethanol solution) and BHNP groups. A subcutaneous injection was administered at a dose of 0.33 mg g^{-1}. Blood samples (400 µL) were collected from the subclavian vein at 0.08, 0.25, 0.5, 1, 2, 4, and 6 h intervals. Samples were collected using heparin-containing tubes (Vacutainer; BD, Franklin Lakes, NJ, USA) and immediately centrifuged at 3000 rpm for 10 min. Plasma was collected and stored at −20 °C. Plasma samples (40 µL) were mixed with 20-µL internal standard solution (carbamazepine 20 µL mL^{-1}) and 1-mL methanol was added to induce protein precipitation. The mixture was centrifuged at 3000 rpm for 10 min, and the supernatant was evaporated under vacuum for 2 h. The final dry residue was resuspended in methanol and analyzed via HPLC. Pharmacokinetic parameters were calculated and predicted utilizing the Phoenix WinNonlin V8.1 software (Certara, St. Louis, MO, USA). The area under the concentration–time curve (AUC$_{0-t}$), C$_{max}$, T$_{max}$, the distribution half-life, elimination half-life (K$_{10}$_HL), and clearance were provided.

Toxicity Assessment

Bagg Albino (BALB/c) mice were subcutaneously administered with doses of 0.33 mg g^{-1}. The mice were treated with the belinostat control and BHNPs for 4 h. 100-µL blood samples were obtained from the tail vein and collected using a heparin-containing tube for subsequent analysis of the complete blood count. Blood samples were analyzed using automated blood analysis (XT-1800i; Sysmex, Kobe, Japan) for erythrocyte, platelet, and total white blood cell counts. Hemoglobin (Hb), RBCs, Hematocrit, mean cell volume, mean cell hemoglobin, and mean corpuscular hemoglobin concentration were also assessed with reference values obtained from the Charles River Laboratory.

Statistical Analysis

All data were analyzed using GraphPad Prism, Version 8. Statistical analyses were performed using the t-test, one-way or two-way analysis of variance, and post hoc Tukey's test. A 0.05-level probability was taken as a significant level. All data are expressed as the mean ± standard deviation.

Results
Optimization and Characterization of HSA NP Delivery System

Belinostat was entrapped into HNPs for optimizing the various factors influencing the manufacturing process. Table 1 shows the particle size, PDI, zeta potential, and the entrapment efficiency of HNPs and BHNPs. HNPs have a size of

Table 1 Physicochemical Characteristics of HNPs and BHNPs

Formulation Code	Particle Size (nm)	Polydispersity Index (PDI)	ζ-Potential (mV)	Encapsulation Efficiency (%)
HNP-50	92.73 ± 03.97	0.23 ± 0.01	−52.98 ± 1.94	NA
BHNP-50	147.47 ± 1.40	0.16 ± 0.04	−53.87 ± 4.81	89.75 ± 0.02
HNP-100	244.43 ±10.25	0.25 ± 0.03	−50.87 ± 1.40	NA
BHNP-100	218.83 ± 4.53	0.15 ± 0.01	−46.22 ± 2.74	89.76 ± 0.12

Notes: HNPs (human serum albumin nanoparticles), BHNPs (belinostat-HNPs), 50 and 100 indicate 50 and 100 mg HSA. Data represented as mean ± SD (n = 3).
Abbreviation: NA, not applicable.

~100 nm with a strong negative charge (−61.98 mV). The sizes of BHNPs slightly increase to 147 nm with nearly the same zeta potential values as those of HNPs. Moreover, the size increases with an increase in the concentration of HSA. The belinostat entrapment efficiency is ~89% and is not influenced by the concentration of HSA.

Figure 2A and B show a range of HNP concentrations in the range of 25–75 mg mL^{-1} with corresponding particle sizes of <200 nm and narrow PDI (<0.2). The size of HNPs increases to 500 even 1300 nm when the HNP content is >100 mg mL^{-1}. Figure 2C shows that the zeta potential of HNPs in the concentration range of 25–125 mg mL^{-1} is negative and lies between −30 and −70 mV, depending on the HNP concentration. A pH range of 4–10 was evaluated to select a suitable pH environment for synthesizing BHNPs. Figure 3A and B show that the sizes of HNPs and BHNPs are relatively small (~100 nm) at pH 6. Moreover, the sizes slightly increase (~200 nm) in the pH range of 6–10.

Thus, 50- and 100-mg HSA were selected and termed HNP-50 and −100, respectively, for further study. Table 1 summarizes the physicochemical properties of HNPs and BHNPs. The average particle size of HNP-50 (92 nm) is smaller than HNP-100 (244 nm). The PDI values of HNP-50 and −100 are similar in the range of 0.23–0.25. The particle sizes of BHNP-50 and −100 are larger, while the PDI values are smaller than those of HNP-50 and −100. Figure 4 shows the morphology of BHNPs as nanometer-sized spheres analyzed via SEM and TEM. Moreover, freeze-dried BHNPs with
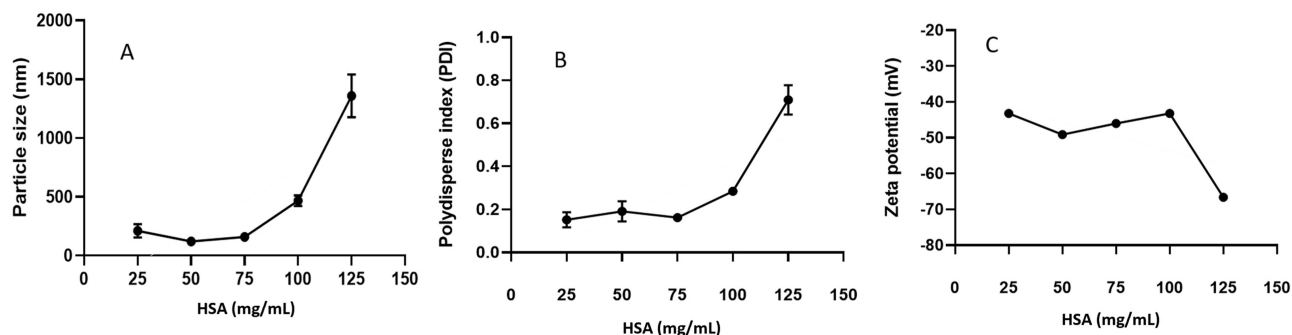
Figure 2 The relationship between HSA concentrations and (**A**) particle size, (**B**) PDI, and (**C**) zeta potential.
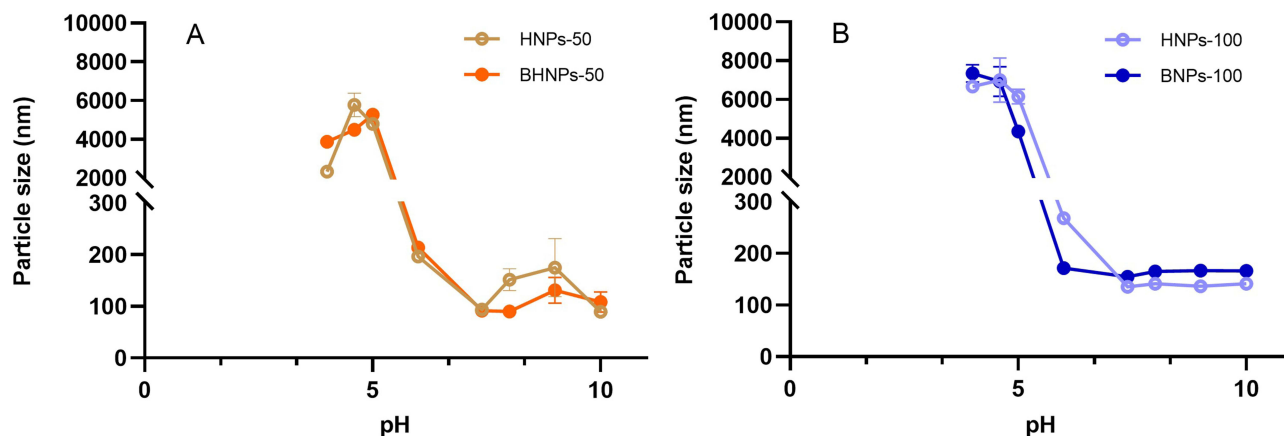
Figure 3 Effect of the particle size at different pH values in HNPs and BHNPs at (**A**) 50 mg/mL, (**B**) 100 mg/mL.
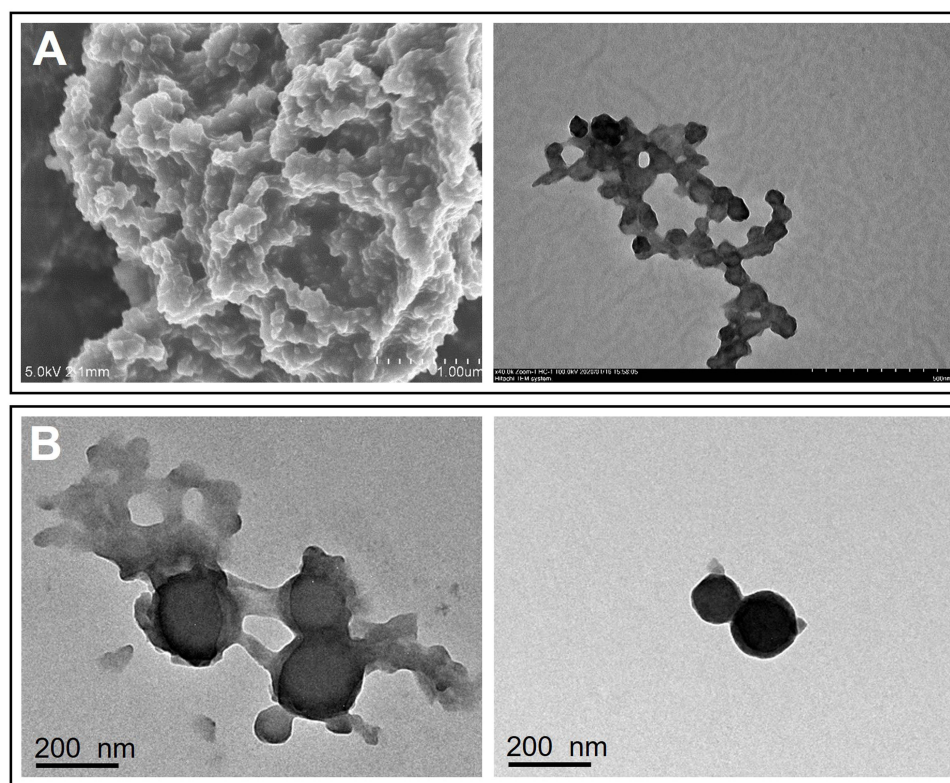
Figure 4 Morphology of BHNPs. (**A**) SEM and (**B**) TEM.

sucrose and trehalose as cryoprotectants can be preserved well. Table 2 shows that 3% sucrose– or trehalose–incorporated BHNPs can maintain a size of <200 nm.

FTIR Characterization

Figure 5 shows the FTIR spectra of belinostat, HNP-50, BHNP-50, and HSA lyophilized powder. The FTIR spectrum of belinostat shows the main peaks of the O–H stretching vibrations of hydroxyacrylamide at 3235 cm^{-1}, the N–H stretching of the secondary amine at 3215 cm^{-1}, the C–H stretching of the aromatic ring at 3040 cm^{-1}, and the S=O stretching of sulfonamide at 1153 and 1340 cm^{-1}. The spectra of HNP-50 and BHNP-50 are similar. The major characteristic absorption bands of belinostat are not present in the spectra of BHNP-50.

Molecular Docking Assay

The intermolecular interaction between belinostat and HSA was analyzed via molecular docking. The binding affinity between belinostat and HSA is −9.5 kcal mol^{-1}. Figure 6 shows that the two aromatic rings of the belinostat molecule are in contact with the active site of HSA through π–π stacking and T-shape interactions with the aromatic ring of Tyr 161 and the Phe 157 side chain, respectively. Two sets of π–alkyl interactions exist between the two aromatic rings of

Table 2 Effect of the Use of Cryoprotectants on the Freeze-Dried Samples

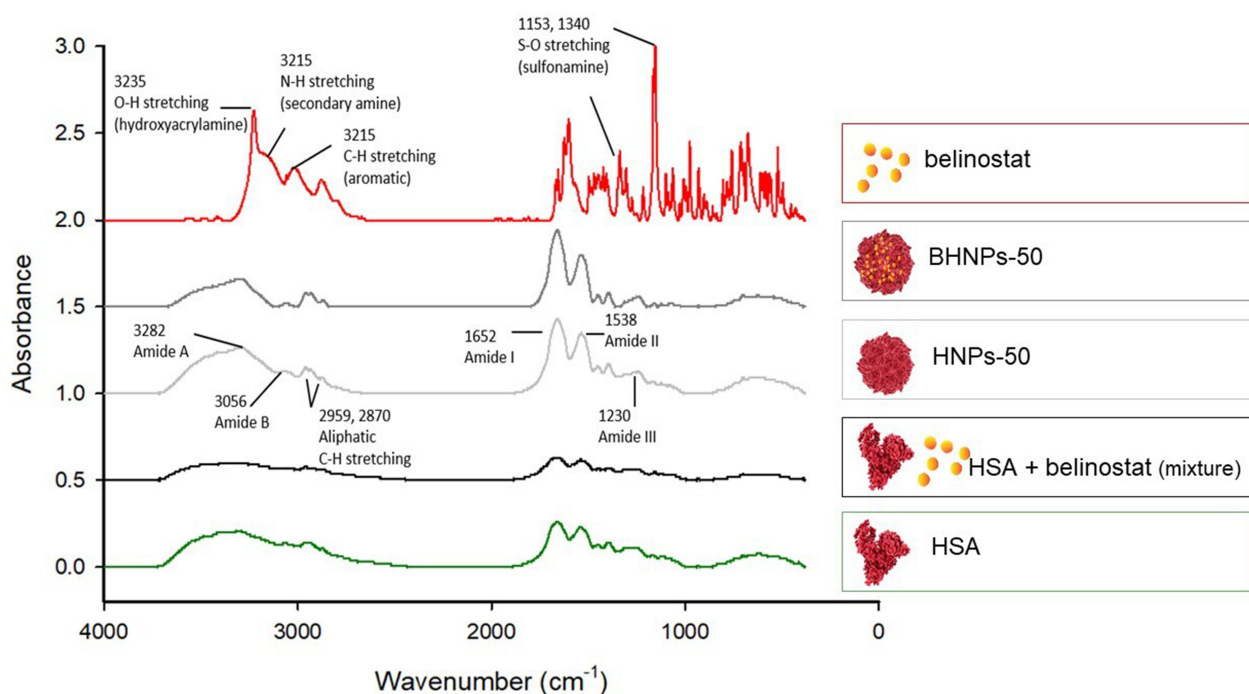| BHNP-50		Size (nm)	PDI
Before freeze dry		147.47 ± 1.40	0.16 ± 0.04
Cryoprotectants	**Sucrose**	184.10 ± 16.72	0.13 ± 0.01
	Trehalose	185.77 ± 45.23	0.18 ± 0.06

Figure 5 FTIR spectra of belinostat, HNP-50, BHNP-50, and HSA lyophilized powder.

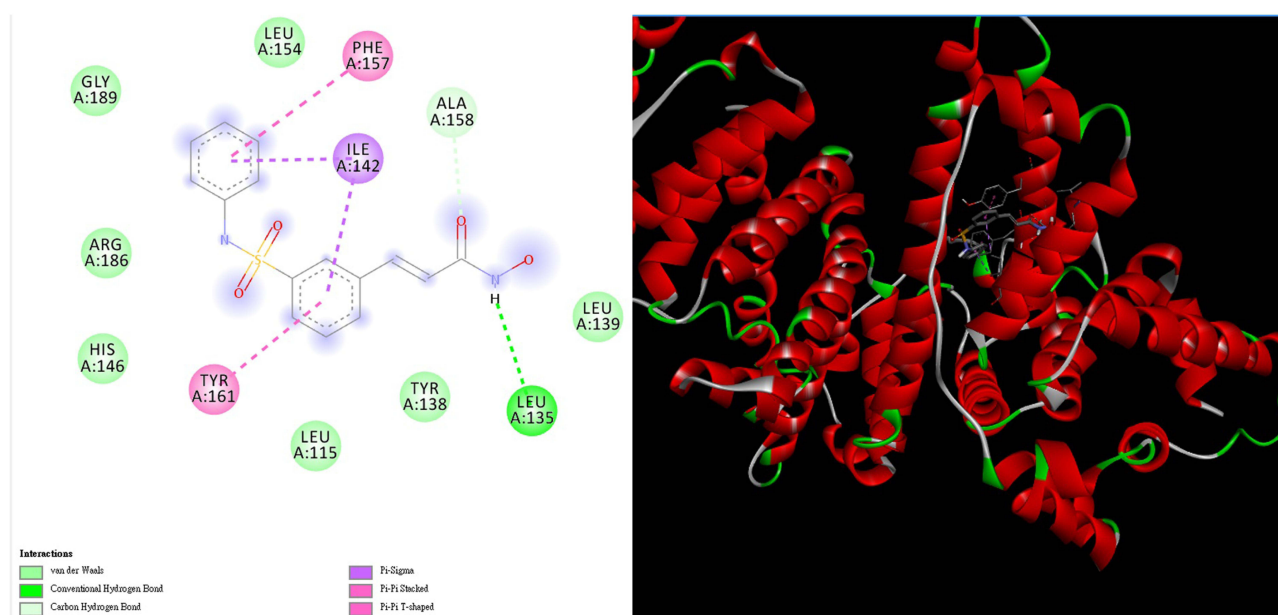**Figure 6** Molecular docking between belinostat and HSA. The binding affinity is −9.5 kcal mol⁻¹.

belinostat and the two methyl groups of the Ile 142 side chain. The H bond between the carbonyl group of belinostat and the α-H on the Ala 158 side chain also induces the binding of the ligand with HSA.

In vitro Cytotoxicity Study

The cytotoxicity results of HuT-78 treatment with HNPs and BHNPs are shown in Figure 7. HNPs maintain a cell viability of ~100% when treated for 24 h. An increase in the treatment time to 48 and 72 h decreases the viability of HuT-78 cells to

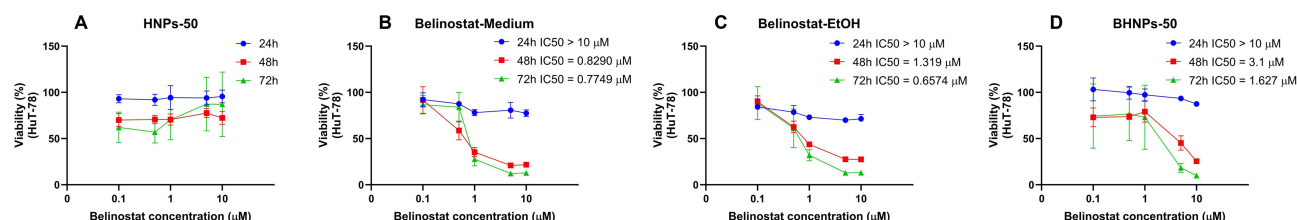**Figure 7** Cytotoxicity of (**A**) HNPs, (**B**) belinostat dissolved in medium, (**C**) belinostat dissolved in EtOH and (**D**) BHNPs on Hut-78 cutaneous T-cell lymphoma cell lines at the concentrations of 0.1–10 μM after treatment for 24, 48, 72 h.

~60%. The HuT-78 cells in the medium and ethanol are highly cytotoxic than belinostat-treated HuT-78 cells for 48 or 72 h. The inhibition of HuT-78 is notable within the concentration range of 1–10 μM. The inhibition of HuT-78 is limited when the dose is >100 μM. HNPs do not inhibit HuT-78 ($p > 0.05$). The IC_{50} of BHNPs after 24 h decreases to 71 μM.

We evaluated the cytotoxicity of PBMCs to understand the influence of immunology (Figure 8). PBMCs are not influenced by HNPs in the range of 10^{-2}–10 μM. The viability of PBMCs decreases on treatment with a belinostat concentration of 10 μM. The viability of PBMCs was higher when treated with BHNPs than that with HNPs. In the case of high-dose treatment groups (100 μM), the viability of PBMC is ~0% and ~50% when treated with HNPs and BHNPs, respectively.

Ex vivo Hemolysis Assay

The ex vivo hemolysis assay was used to evaluate the biocompatibility of BHNPs with blood for intravenous administration. Figure 9 shows no hemoglobin in sample bottles containing BHNP-treated samples. Moreover, the hemoglobin levels of BHNP-50 and −100 are 2% and 4%, respectively.

In vivo Toxicity Assessment

The complete blood counts after treatment with belinostat and BHNPs were analyzed via in vivo animal toxicity studies. Table 3 shows that the results of the belinostat-treated group are similar to those of the BHNP-treated group, except for the platelet count. The platelet count of the belinostat-treated group ($p < 0.05$) is significantly lower than the reference. However, the BHNP-treated group shows a platelet count in the reference range.

In vivo Pharmacokinetics

The plasma drug concentration–time curve of HNPs and BHNPs after subcutaneous administration and the relevant pharmacokinetic parameters are shown in Figure 10 and Table 4, respectively. The observed T_{max} and C_{max} values of BHNPs are higher than those of belinostat ($p < 0.05$). Moreover, the AUC of BHNPs is slightly higher (77.53 h* μg mL^{-1}) than that of belinostat (61.9777.53 h μg mL^{-1}). The K10-HL, distribution and elimination half-life, of BHNPs is slightly slower than HNPs ($p > 0.05$).
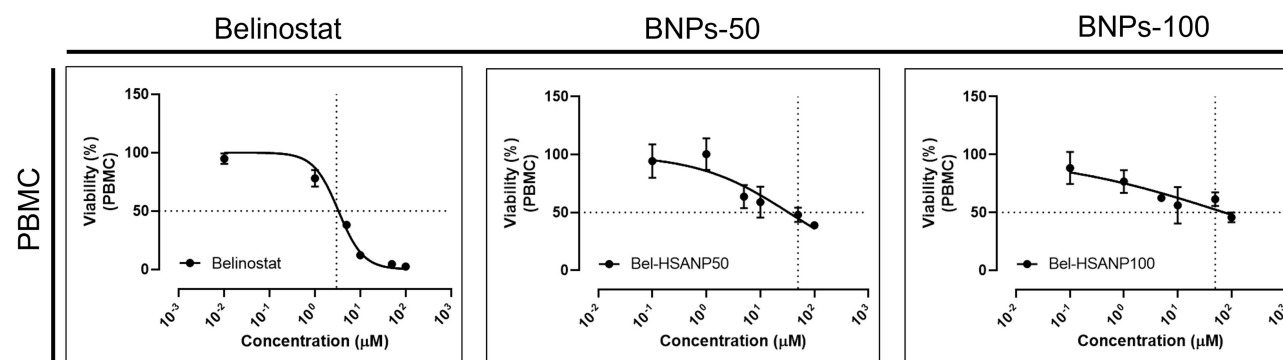

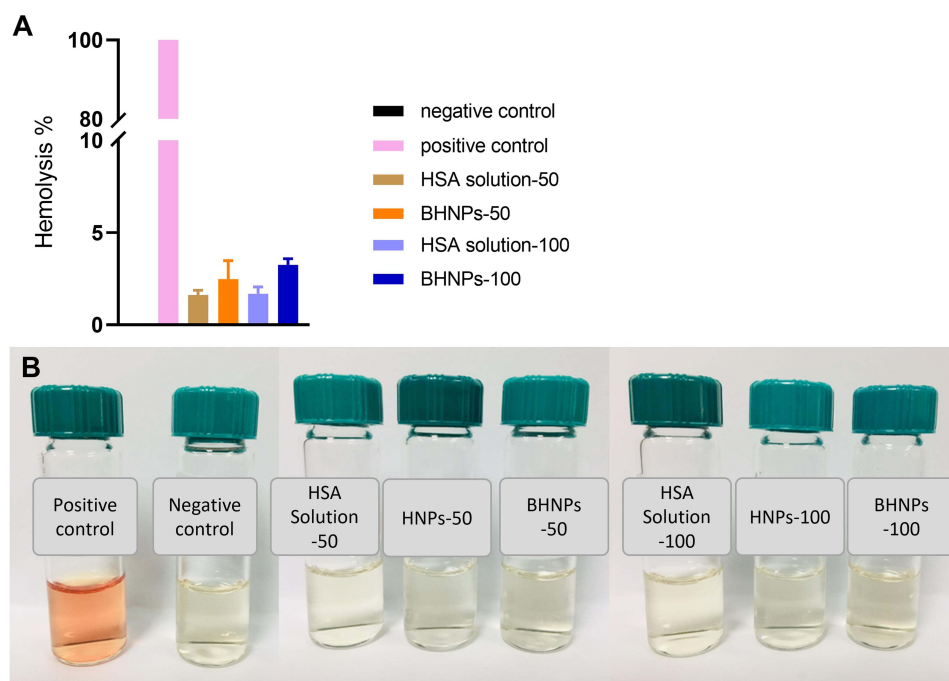**Figure 8** In vitro cytotoxicity of PBMCs on treatment with belinostat and BHNPs.

Figure 9 In vitro hemolysis of male SD rat erythrocytes induced by HNPs and BHNPs. (**A**) UV detection and (**B**) observation.

Discussion

Belinostat is a potent histone deacetylase inhibitor used in cancer therapy. However, poor solubility, rapid degradation, and adverse side effects like thrombocytopenia have limited its clinical application. To solve this problem, human serum albumin nanoparticles were used as a delivery system. Belinostat was successfully incorporated into HNPs, forming homogeneous, negatively charged nanoparticles (~150 nm). The results demonstrated that BHNPs exhibited dose-dependent cytotoxicity comparable to free Belinostat, confirming their effectiveness in targeting cancer cells. Notably, BHNPs displayed reduced toxicity towards PBMCs, providing protection to normal cells. Furthermore, in vivo toxicology assessments showed that BHNPs can improve the adverse reaction of thrombocytopenia. These findings suggest that BHNPs maintain the anticancer activity against HuT-78 cells while offering a safer profile by minimizing to normal immune cells (PBMCs), making them a promising option for reducing adverse effects during the treatment period.

Desolvation method is a common method to prepare the human serum albumin nanoparticles. It provided the stable nanoparticles and good encapsulation efficiency. In the pharmaceutical industry, high-pressure homogenization was used

Table 3 In vivo Toxicity Assessment Comparing Complete Blood Counts (CBC) in BALB/c Mice After Intraperitoneal Injection of Belinostat and BHNPs with a Dose of 0.333 mg G^{-1}

Items	Blank	Belinostat Control	BHNP-50	Reference Values
WBC count (10^9 L^{-1})	3.13 ± 0.62	3.56 ± 0.32	4.10 ± 1.25	3.48–14.03
RBC count (10^{12} L^{-1})	9.45 ± 0.41	7.37 ± 0.75	7.92 ± 1.28	6.93–12.24
Hb (g dL^{-1})	13.9 ± 0.38	13.20 ± 1.06	12.30 ± 1.90	12.60–20.50
Hct (%)	51.10 ± 0.80	45.30 ± 5.28	43.53 ± 9.00	42.10–68.30
MCV (fL)	55.47 ± 0.70	54.73 ± 0.35	53.67 ± 1.27	41.50–57.40
MCH (pg)	15.40 ± 0.20	15.57 ± 0.46	15.47 ± 0.06	14.10–18.40
MCHC (%)	27.1 ± 0.10	28.50 ± 0.70	29.00 ± 0.87	23.30–32.70
Plt (10^9 L^{-1})	623± 105.16	235.32 ± 34.21*	458.00 ± 52.36	420–1698

Note: Data are shown as mean ± SD (n = 3).
Abbreviations: WBC, white blood cell; RBC, red blood cell; Hb, hemoglobin; Hct, hematocrit; MCV, mean cell volume; MCH, mean cell hemoglobin; MCHC, mean corpuscular hemoglobin concentration; Plt, platelet.
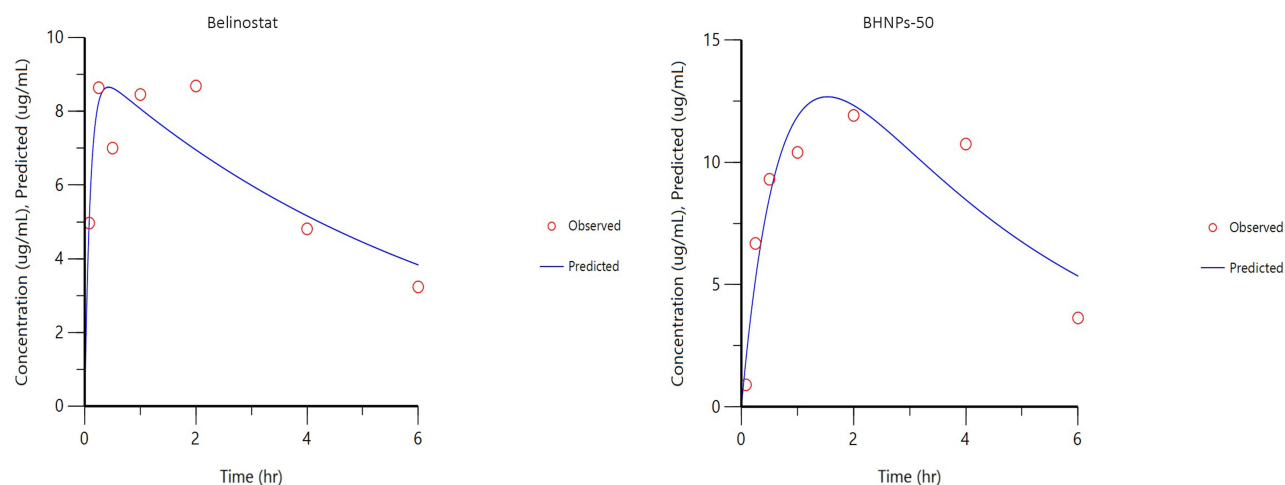
Figure 10 Plasma concentration vs time profile of the pharmacokinetic behavior of belinostat and BHNPs after subcutaneous administration in Balb/c mice at a single dose of 0.333 mg g^{-1} obtained using first-order kinetic calculation.

as methods for manufacturing human serum albumin nanoparticles. However, the batch size of the high-pressure homogenizer varied between 40 mL and 50 L, which was a limitation in the lab-scale setup.[28] The size of BHNP-50 and BHNP-100 particles is controlled in the range of 147–218 nm to incorporate belinostat. The PDI of BHNPs slightly decreases with higher entrapment efficiency (90%) than those of HNPs, suggesting that belinostat and HSA have good fusion capability. Molecular docking is a valuable tool for obtaining structure-based information through protein modeling and ligand docking. Molecular docking studies reveal that belinostat interacts through π–π stacking and T-shape interaction with HSA. Moreover, π–alkyl interaction binds belinostat to HSA. Belinostat successfully assembles in HNPs owing to its high protein-binding property to form BHNPs. A suitable drug carrier increases self-assembly and entrapment efficiency.

Different concentrations of HSA affect particle sizes. Thus, we examined a range from unsaturated to supersaturated concentrations of HSA to identify a suitable range between belinostat and HSA. A concentration ranges of 25–100 mg mL−1 of HSA with suitable nanoscale particle sizes (<500 nm) was used for the preparation of BHNPs. Our findings demonstrate that significant aggregation phenomena are clearly observed at pH values below 6.0. When pH values higher than 6.0, the nanoparticles were well dispersed.[29] Previous research had similar results, monodisperse particles between 200 and 300 nm could be prepared at pH 8.0 and above. Precipitation was rationalized based on the isoelectric point. Albumin molecules aggregate as the pH approaches the isoelectric point of albumin (4.7), attributed to a nearly neutral net charge. The HSA concentrations of 50 and 100 mg mL^{-1} were selected for BHNP preparation with a pH ~ 7

Table 4 In vivo Pharmacokinetic Parameter Comparison in SD Rats After Subcutaneous Injections with a Dose of 0.333 Mg G^{-1} Between Belinostat and BHNPs

PK Parameters	Belinostat Control	BHNP-50
AUC$_{0-t}$ (h μg mL^{-1})	61.97 ± 28.71	77.53 ± 20.30
Cmax (μg mL^{-1})	8.65 ± 0.78	12.67 ± 1.39*
Tmax (h)	0.43 ± 0.13	1.53 ± 0.30*
K10_HL (h)	4.66 ± 1.66	2.96 ± 1.57
CL (mL h^{-1})	5.32 ± 1.53	4.26 ± 1.12

Notes: Data are presented as mean ± standard deviation (n = 3). *p < 0.05 was considered statistically significant.
Abbreviations: AUC, area under curve; Cmax, maximum concentration observed; Tmax, Time of maximum concentration observed; K10_HL, the distribution half-life and elimination half-life; Cl, clearance.

(unadjusted albumin solution), ethanol/albumin solution volume ratio of 2, and ethanol at a rate of 0.5 mL min−1 as the critical preparation parameters based on the evaluation and previous tests.

The nanoparticle surface charge is an important parameter in stability and binding behavior for targeting drug delivery. BHNPs have a negative charge of ∼−50 mV, indicating that BHNPs have a high affinity to interact with the cellular membrane via electrostatic forces. An electrostatic force maintains a distance, which prevents the aggregation of HNPs.[30] Previous studies indicate that negatively charged particles can also be rapidly ionized and massively cleared by fixed macrophages.[31] Moreover, negatively charged nanoparticles would attract plasma proteins such as albumins and fibronectin, which play a crucial role in influencing their biological behavior, particularly regarding how they are internalized by cells.[32] Particularly in cancer therapy, the characteristic acts as diversity function. On one side, it can enhance targeted delivery to cancer cells by enhancing nanoparticle uptake, but on the other, it increases the potential for recognition and uptake by macrophages, resulting in quicker clearance from the body. The surface charge is a determining factor in this process, with negatively charged NPs generally being more effective at avoiding opsoniza-tion, the immune system's process for marking foreign entities for clearance.[33] FTIR is used for investigating the conformational analysis of proteins, especially to provide secondary structure information. The secondary structure of HSA is denatured during heating.[34] Thus, we analyzed BHNPs via FTIR to investigate the entrapment of belinostat into HNPs. Amide I (–CO–NH–) bands (1700–1600 cm^{-1}) are the most prominent vibrational bands of the protein backbone, indicating protein secondary structure.[35] Amide I absorption bands in the range of 1600–1800 cm^{-1} are present in HNPs and BHNPs, indicating that the secondary structure is intact during the synthesis. The major functional groups hydroxyacrylamide (N–H, 3325 cm^{-1}) and sulfonamide (S=O, 1153 and 1340 cm^{-1}) of belinostat are not present in BHNPs, indicating that those belinostat molecules are entrapped into HNPs. The disappearance of these characteristic functional group peaks suggests that belinostat molecules were encapsulated rather than simply adsorbed onto the surface of the nanoparticles.

The freeze dying process is an important strategy to remove water from the sample via sublimation, especially for heat-sensitive materials or protein-based materials to increase the storage period. Thus, sucrose and trehalose were selected as cryoprotectants suitable for the protein-based formula, as nonreducing compounds can avoid the potential Maillard reaction between the excipient and protein.[36] Sucrose and trehalose controlled the size of BHNPs in the desired nanoscale. They stabilized BHNPs by preventing aggregation.

Belinostat, a powerful chemotherapeutic drug, has a strong concentration-dependent character when dissolved in a medium or ethanol. We designed different vehicles for dissolution to elucidate the impact of solubility on cytotoxicity. Belinostat dissolved in ethanol with a marginal variation decreases the IC_{50} value fourfold after short-term exposure (24 h), indicating that the solubility of belinostat might be a contributing factor. Cytotoxicity is similar after 48 and 72 h with a slight difference in the IC_{50} value. The IC_{50} of the BHNP group is higher than that of the belinostat groups. Thus, a low dose and treatment time are required for the BHNP group, and it has high cytotoxicity. Previous studies suggest that drug molecules are either encapsulated within or adsorbed onto the surface of HSANPs. This interaction can limit the immediate release of the drug, often requiring specific stimuli such as pH changes or enzymatic degradation to initiate effective drug release.[37]

A comparison with our previous results indicates that the cytotoxic activity of belinostat-loaded liposomes was better than that of BHNPs.[38] The selection of a suitable candidate is an important issue during the development of the preformulation stage. HNPs can target specific tumor cells, which reduces drug toxicity.[39] HNPs exhibit increased safety as chemotherapeutic agents in high doses. Selecting a suitable carrier for drug delivery is a crucial step in the early drug development process. Several factors are considered while selecting a suitable carrier for drug delivery: carrier characteristics, bioavailability, solubility, release rate, stability, and preparation techniques. The carrier should be compatible with the drug characteristics to ensure an effective delivery.

An in vitro cellular study was conducted to investigate the safety of the drug carrier. PBMCs are critical cells for determining the dosage limit of new drugs.[40] BMCs refer to monocytes and lymphocytes, representing the cells of the innate and adaptive immune systems.[41] Hence, PBMC was used as an assessment model to understand the influence of immunology. Although the viability of PBMCs is not different between belinostat and BHNPs, the BHNP-treated group shows 50% survival of PBMCs. However, the belinostat-treated group shows no survival at the same dose treatment

(100 μM). Thus, HNPs as carriers would be safer than liposome-loaded belinostat in PBMC, despite the cytotoxicity of BHNPs being slightly less than that of the liposome-loaded belinostat. The administration of a high concentration of belinostat is possible using BHNPs with enhanced safety within PBMCs.

The results of the in vivo toxicology assessment show that the belinostat group has a lower blood platelet count than the reference value. Low blood platelet count (thrombocytopenia) is the most common Grade 3 to 4 (~7%) and ~16% of all grades adverse events of belinostat. Thrombocytopenia is an adverse reaction commonly observed in HDAC inhibitors, such as romidepsin, vorinostat, panobinostat, and belinostat.[42] These symptoms are relevant to two common polymorphisms (UGT1A1*28 and UGT1A1*60), which are associated with impaired drug clearance and thrombocytopenia risk, probably owing to increased drug exposure.[43]

Previous reports of population pharmacokinetic (PPK) studies demonstrated that platelet levels were recovered within 21 days in cancer patients before the next cycle of therapy.[43] Cody et al also suggested that thrombocytopenia is caused by high belinostat exposure. This adverse reaction is owing to the dose response of belinostat. Thrombocytopenia can be inhibited by eliminating the drug from the body. Previous trial reports indicated that belinostat can be safely administered to patients with a platelet count >25,000 μL^{-1} without requiring any dosage adjustment.[44] The toxicity assessment results indicate that BHNPs can reverse the thrombocytopenia of HDAC inhibitors. The administration of BHNPs increases the blood platelet value to reach the normal reference value. Thus, the adverse reaction of blood platelets can be improved by using HNP carriers. Moreover, BHNPs do not require dosage adjustment, providing additional safety to patients.

The pharmacokinetic profile and parameters of the belinostat and BHNP groups are illustrated in Figure 10 and Table 3. The Cmax and AUC values of the BHNP group are higher than those of the belinostat group, indicating the sustained drug release ability and long duration in circulation ($p < 0.05$). The elimination of the half-life of the BHNP group is slower than that of the belinostat group, suggesting that BHNPs are eliminated from the blood at a slow rate. The findings of this study provide important insights into the pharmacokinetic profile and parameters of BHNPs, which might boost the development of a novel drug-delivery system. The application of the HNP system in this study effectively delivers belinostat into blood, resulting in an extended circulation time and a slow elimination rate.

Conclusion

Belinostat, an HDAC inhibitor, is a chemotherapeutic agent for various hematological cancers. However, its use is limited by the thrombocytopenia symptom, especially at higher doses. Its poor solubility and short half-life restrict its distribution and administration. We exploited nanomedicine strategies in this study. We selected HSA, a biomimetic material with excellent compatibility and low immunogenicity, ideal for self-binding owing to its high protein-binding interaction force. We successfully prepared BHNPs with a nanoscale size of 150 nm and high entrapment efficiency. BHNPs demonstrated a predominant cytotoxicity for HuT-78 at a low concentration over 24, 48, and 72 hrs. Moreover, BHNPs had a high tolerance to PBMCs, indicating that BHNPs are safe at high concentrations. BHNPs showed a minimum hemolysis. Pharmacokinetic analyses revealed that BHNPs exhibited sustained release and prolonged circulation. Importantly, BHNPs reverse thrombocytopenia associated with HDAC inhibitors also provide a safer drug delivery system without the need for dosage adjustment. Our findings suggest that BHNPs represent a promising approach to reduce adverse reactions associated with belinostat, potentially offering a safer treatment option for hematological cancers.

Acknowledgments

Disclosure

The authors declare no conflict of interest.

References

1. Amer W, Amitava D. Chapter 12 - T cell and natural killer cell lymphomas. In: Amer W, Amitava D, editors. *Hematology and Coagulation: A Comprehensive Review for Board Preparation, Certification and Clinical Practice*. Elsevier; 2015:199–214.

2. Laribi K, Alani M, Truong C, Baugier de Materre A. Recent advances in the treatment of peripheral T-cell lymphoma. *Oncologist*. 2018;23 (9):1039–1053. doi:10.1634/theoncologist.2017-0524

3. Eckschlager T, Plch J, Stiborova M, Hrabeta J. Histone deacetylase inhibitors as anticancer drugs. *Int J Mol Sci*. 2017;18(7):1414. doi:10.3390/ijms18071414

4. Yoon S, Eom GH. HDAC and HDAC inhibitor: from cancer to cardiovascular diseases. *Chonnam Med J*. 2016;52(1):1–11. doi:10.4068/cmj.2016.52.1.1

5. Patel VK, Shirbhate E, Tiwari P, et al. Multi-targeted HDAC inhibitors as anticancer agents: current status and future prospective. *Curr Med Chem*. 2023;30(24):2762–2795. doi:10.2174/0929867329666220922105615

6. Peer CJ, Goey AK, Sissung TM, et al. UGT1A1 genotype-dependent dose adjustment of belinostat in patients with advanced cancers using population pharmacokinetic modeling and simulation. *J Clin Pharmacol*. 2016;56(4):450–460. doi:10.1002/jcph.627

7. Yeo W, Chung HC, Chan SL, et al. Epigenetic therapy using belinostat for patients with unresectable hepatocellular carcinoma: a multicenter phase I/II study with biomarker and pharmacokinetic analysis of tumors from patients in the mayo phase II consortium and the cancer therapeutics research group. *J Clin Oncol*. 2012;30(27):3361–3367. doi:10.1200/JCO.2011.41.2395

8. Urbinati G, Marsaud V, Plassat V, Fattal E, Lesieur S, Renoir JM. Liposomes loaded with histone deacetylase inhibitors for breast cancer therapy. *Int J Pharm*. 2010;397(1–2):184–193. doi:10.1016/j.ijpharm.2010.06.046

9. Xiao K, Li YP, Wang C, et al. Disulfide cross-linked micelles of novel HDAC inhibitor thailandepsin A for the treatment of breast cancer. *Biomaterials*. 2015;67:183–193. doi:10.1016/j.biomaterials.2015.07.033

10. Tran TH, Choi JY, Ramasamy T, et al. Hyaluronic acid-coated solid lipid nanoparticles for targeted delivery of vorinostat to CD44 overexpressing cancer cells. *Carbohydr Polym*. 2014;114:407–415. doi:10.1016/j.carbpol.2014.08.026

11. Liao H, Zhao S, Wang H, Liu Y, Zhang Y, Sun G. Self-assembly of retinoid nanoparticles for melanoma therapy. *Int J Nanomed*. 2019;14:7963–7973. doi:10.2147/IJN.S196974

12. Ma W, Sun J, Xu J, et al. Sensitizing triple negative breast cancer to tamoxifen chemotherapy via a redox-responsive vorinostat-containing polymeric prodrug nanocarrier. *Theranostics*. 2020;10(6):2463–2478. doi:10.7150/thno.38973

13. Godeshala S, Miryala B, Dutta S, et al. A library of aminoglycoside-derived lipopolymer nanoparticles for delivery of small molecules and nucleic acids. *J Mater Chem B*. 2020;8(37):8558–8572. doi:10.1039/d0tb00924e

14. Bertrand P, Blanquart C, Heroguez V. The ROMP: a powerful approach to synthesize novel pH-sensitive nanoparticles for tumor therapy. *Biomolecules*. 2019;9(2):60. doi:10.3390/biom9020060

15. Anselmo AC, Mitragotri S. Nanoparticles in the clinic: an update. *Bioeng Transl Med*. 2019;4(3):e10143. doi:10.1002/btm2.10143

16. Solanki R, Rostamabadi H, Patel S, Jafari SM. Anticancer nano-delivery systems based on bovine serum albumin nanoparticles: a critical review. *Int J Biol Macromol*. 2021;193(Pt A):528–540. doi:10.1016/j.ijbiomac.2021.10.040

17. Sleep D. Albumin and its application in drug delivery. *Expert Opin Drug Deliv*. 2015;12(5):793–812. doi:10.1517/17425247.2015.993313

18. Lee P, Wu X. Review: modifications of human serum albumin and their binding effect. *Curr Pharm Des*. 2015;21(14):1862–1865. doi:10.2174/1381612821666150302115025

19. White J, Laux V, Fraser N, Hess D, Haertlein M, Forsyth T. Deuterium effects on human serum albumin in solution. *Physica B*. 2018;551:208–211. doi:10.1016/j.physb.2018.01.065

20. An FF, Zhang XH. Strategies for preparing albumin-based nanoparticles for multifunctional bioimaging and drug delivery. *Theranostics*. 2017;7 (15):3667–3689. doi:10.7150/thno.19365

21. Zhang Y, Sun T, Jiang C. Biomacromolecules as carriers in drug delivery and tissue engineering. *Acta Pharm Sin B*. 2018;8(1):34–50. doi:10.1016/j.apsb.2017.11.005

22. Hoogenboezem EN, Duvall CL. Harnessing albumin as a carrier for cancer therapies. *Adv Drug Deliv Rev*. 2018;130:73–89. doi:10.1016/j.addr.2018.07.011

23. Abdallah M, Müllertz OO, Styles IK, et al. Lymphatic targeting by albumin-hitchhiking: applications and optimization. *J Control Release*. 2020;10 (327):117–128. doi:10.1016/j.jconrel.2020.07.046

24. Qi S, Wang X, Chang K, et al. The bright future of nanotechnology in lymphatic system imaging and imaging-guided surgery. *J Nanobiotechnology*. 2022;20(1):24. doi:10.1186/s12951-021-01232-5

25. Celgene Corporation. Instructions of Abraxane®. U.S. Food and Drug Administration. Available from: https://www.accessdata.fda.gov/drugsatfda_docs/label/2012/021660s031lbl.pdf. Accessed October 17, 2024.

26. Lodhi NA, Park JY, Kim K, et al. Development of (99m)Tc-labeled human serum albumin with prolonged circulation by chelate-then-click approach: a potential blood pool imaging agent. *Mol Pharm*. 2019;16(4):1586–1595. doi:10.1021/acs.molpharmaceut.8b01258

27. Patel K, Jain P, Rajput PK, et al. Human serum albumin-based propulsive piperlongumine-loaded nanoparticles: formulation development, characterization and anti-cancer study. *Colloids Surf A Physicochem Eng Asp*. 2022;652(5):129738. doi:10.1016/j.colsurfa.2022.129738

28. Jenning V, Lippacher A, Gohla SH. Medium scale production of solid lipid nanoparticles (SLN) by high pressure homogenization. *J Microencapsul*. 2002;19(1):1–10. doi:10.1080/713817583

29. Langer K, Anhorn MG, Steinhauser I, et al. Human serum albumin (HSA) nanoparticles: reproducibility of preparation process and kinetics of enzymatic degradation. *Int J Pharm*. 2008;347(1–2):109–117. doi:10.1016/j.ijpharm.2007.06.028

30. Bernfield M, Gotte M, Park PW, et al. Functions of cell surface heparan sulfate proteoglycans. *Annu Rev Biochem*. 1999;68:729–777. doi:10.1146/annurev.biochem.68.1.729

31. Honary S, Zahir F. Effect of zeta potential on the properties of nano-drug delivery systems—a review (Part 1). *Trop J Pharm Res*. 2013;12 (2):255–264. doi:10.4314/tjpr.v12i2.19

32. Singh N, Marets C, Boudon J, Millot N, Saviot L, Maurizi L. In vivo protein Corona on nanoparticles: does the control of all material parameters orient the biological behavior? *Nanoscale Adv*. 2021;3(5):1209–1229. doi:10.1039/d0na00863j

33. Bashiri G, Padilla MS, Swingle KL, Shepherd SJ, Mitchell MJ, Wang K. Nanoparticle protein Corona: from structure and function to therapeutic targeting. *Lab Chip*. 2023;23(6):1432–1466. doi:10.1039/d2lc00799a

34. Usoltsev D, Sitnikova V, Kajava A, Uspenskaya M. Systematic FTIR spectroscopy study of the secondary structure changes in human serum albumin under various denaturation conditions. *Biomolecules*. 2019;9(8):359. doi:10.3390/biom9080359

35. Yang H, Yang S, Kong J, Dong A, Yu S. Obtaining information about protein secondary structures in aqueous solution using Fourier transform IR spectroscopy. *Nat Protoc*. 2015;10(3):382–396. doi:10.1038/nprot.2015.024

36. Chang L, Shepherd D, Sun J, et al. Mechanism of protein stabilization by sugars during freeze-drying and storage: native structure preservation, specific interaction, and/or immobilization in a glassy matrix? *J Pharm Sci*. 2005;94(7):1427–1444. doi:10.1002/jps.20364

37. Kratz F. Albumin as a drug carrier: design of prodrugs, drug conjugates, and nanoparticles. *J Control Release*. 2008;132(3):171–183. doi:10.1016/j.jconrel.2008.05.010

38. Cheng MH, Weng J-Y, Chuang C-H, et al. Prolonging the half-life of histone deacetylase inhibitor belinostat via 50 nm scale liposomal subcutaneous delivery system for peripheral T-cell lymphoma. *Cancers*. 2020;12(9):2558. doi:10.3390/cancers12092558

39. Trynda-Lemiesz L. Paclitaxel-HSA interaction. Binding sites on HSA molecule. *Bioorg Med Chem*. 2004;12(12):3269–3275. doi:10.1016/j.bmc.2004.03.073

40. Gill PK. Rapid isolation of peripheral blood mononuclear cells from whole blood with ficoll hypaque density centrifugation. *J Int Res Med Pharm Sci*. 2019;14(1):17–20.

41. de Mello VD, Kolehmanien M, Schwab U, Pulkkinen L, Uusitupa M. Gene expression of peripheral blood mononuclear cells as a tool in dietary intervention studies: what do we know so far? *Mol Nutr Food Res*. 2012;56(7):1160–1172. doi:10.1002/mnfr.201100685

42. Sermer D, Pasqualucci L, Wendel HG, Melnick A, Younes A. Emerging epigenetic-modulating therapies in lymphoma. *Nat Rev Clin Oncol*. 2019;16(8):494–507. doi:10.1038/s41571-019-0190-8

43. Peer CJ, Hall OM, Sissung TM, et al. A population pharmacokinetic/toxicity model for the reduction of platelets during a 48-h continuous intravenous infusion of the histone deacetylase inhibitor belinostat. *Cancer Chemother Pharmacol*. 2018;82(3):565–570. doi:10.1007/s00280-018-3631-7

44. Reddy N, Bodiford A, Talbott M. Critical appraisal of belinostat in the management of T-cell lymphoma–patient considerations. *Blood Lymphat Cancer*. 2015;2015:109. doi:10.2147/BLCTT.S72496